

Supplementary information

1 SP2 data processing

Analysis of single particle data measured by the SP2 involves the examination of each detector signal as a function of time. The large volume of data generated by the instrument requires multiple analysis routines to classify the particle events, but we also performed a visual inspection of random particle events during each flight to verify the performance of the instrument and analysis routines. Liu *et al.* (2010) give a more detailed description of the analysis method for the U. of Manchester SP2, which we only summarize. All SP2 data were averaged over the AMS sampling interval (approximately 30 seconds) for comparison with other aerosol composition data.

The SP2 recorded data every $0.2 \mu\text{s}$ for any event that met triggering thresholds for either scattering or high-gain incandescing detector responses. Particle events were classified as BC-containing if they exceeded the signal threshold for incandescence. Particles that exceeded only the scattering signal threshold were classified as non-BC scattering particles. We fitted a Gaussian curve to the scattering signal for each scattering particle and converted the fitted peak height to particle diameter using the PSL calibration data. If the scattering signal saturated the detector, a Gaussian curve was fitted using the leading edge only (LEO) method of Gao *et al.* (2007). The position of the particle relative to the laser beam must be known, which was determined using the response from the split APD detector. The position of the split was determined from the median value of the last 200 non-saturated, scattering particles measured, which accounted for any drifts in its position observed during PSL calibrations during or between flights.

We calculated the peak height response of each incandescence channel to BC-containing particles by subtracting the signal baseline (the average of the first 6 data points ($1.2 \mu\text{s}$) of the signal) from the maximum signal recorded. The incandescence channel response was converted to particle mass using the Aquadag calibration data. The mass of each incandescing particle was also converted to diameter assuming it was spherical with a density of 1.8 g cm^{-3} (Moteki *et al.*, 2007; Shiraiwa *et al.*, 2008). Sizing information was available from both incandescence channels, resulting in two number and mass distributions. Figure 1 shows an example of number and mass frequency distributions obtained using each incandescence channel, measured for an approximately 5-minute period of the B363 (5 May 2008) flight over western Europe. Both channels return similar distributions between approximately 80-120 nm. Above this size range the high-gain, broadband detector saturates, so no sizing information is available. Below this range the low-gain, narrowband detector response is noisy and the calibration more uncertain (due to the power-law relationship between SP2 signal and BC mass) and there is a disagreement between the broad- and narrowband number distributions. The diameters assigned to single particles by each calibration and detector are not identical; they vary due to differences in the thermal emission spectra (colour ratio) and uncertainty in the fits to calibration data used to assign the diameters. For this reason, we cannot simply assign a single diameter to each particle. Instead we average the distributions measured by each detector, weighting the average towards the high-gain detector at small sizes (where the low-gain detector calibration is uncertain) to

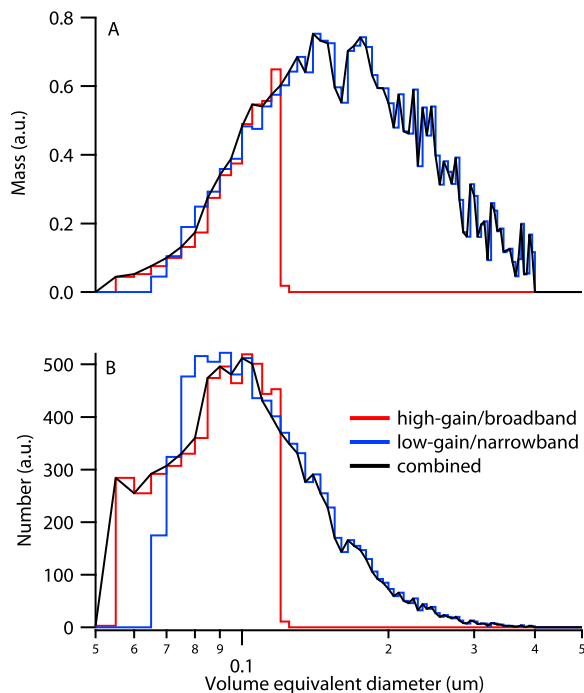


Figure 1: Black carbon mass (a) and number (b) frequency distributions for an approximately 5-minute segment of flight B363 (5 May 2008). High-gain/broadband incandescence detector measured distributions are shown in red, low-gain/narrowband-measured distributions are shown in blue, and the linearly weighted, combined distributions are shown in black.

the low-gain detector at large sizes (where the high-gain detector is saturated). The resulting combined size distributions are also shown in Figure 1. Any mention of BC number and mass distributions in the remainder of this work refers to size distributions combined in this way.

In addition to valid single particles SP2 data events can include: a) anomalous signals resulting from recirculation of particles in the optical cavity, unusual particle shapes, or other unknown factors, b) particles outside the calibration range of the incandescence or scattering detectors (including saturated events) and c) multiple particles within the measurement region (coincident events). The processing routine removes events that do not meet thresholds for scattering or incandescence signals determined from visual inspection of single particle data. Saturated incandescence particles are included in the number concentration measurement, but not included in the mass measurement. The largest of two or more coincident incandescence signals is used in the mass calculation. Scattering particles with LEO fit diameters larger than the largest available PSL calibration size are included in the scattering number concentration, but not in any size-dependent calculations, including aerosol volume concentrations.

The SP2 is also sensitive to other materials that absorb light at 1064 nm, which includes metals. Schwarz *et al.* (2006) compared the broadband/narrowband response ratios measured for several laboratory-generated standard aerosols and ambient aerosol. They found that the distribution of ambient BC ratios did not overlap significantly with the peaks for non-BC ma-

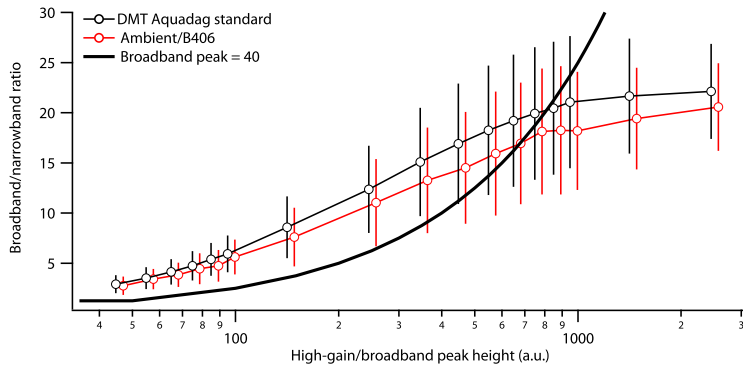


Figure 2: Average SP2 broadband/narrowband detector peak ratios as a function of broadband detector peak height for ambient particles measured during a 10-minute segment of B406 (25 September 2008) and average broadband/narrowband ratios measured for Aquadag calibration particles by the instrument manufacturer. Error bars give \pm one standard deviation for each data set and the ambient data have been slightly offset to the right to better distinguish the points and variability.

terial (chromium, silicon and niobium). We compared the broadband/narrowband ratios measured for the Aquadag calibration particles to ambient measurements from the campaign and found similar agreement between the calibration BC and ambient particles. Figure 2 shows the broadband/narrowband ratios measured for individual particles sampled during the B406 (25 September 2008) flight over the UK as a function of the broadband detector response. The average and standard deviation of the ratios measured during the Aquadag calibration are also shown for comparison. The bulk of the ambient measurements fall within one standard deviation of the mean of the Aquadag ratios, so we treat all incandescing material detected by the instrument as BC. The decrease in the ratio for smaller signals is partly due to low-gain detector signals approaching the noise level of the detector. This is illustrated by the curve showing the maximum ratio expected for a low-gain detector signal of 40 (which we take as the lower signal limit of the detector), shown in Figure 2. Signal ratios falling above this curve have low-gain detector signals below the noise limit of the detector, and should be viewed with caution.

Previous SP2 studies have estimated BC mass outside the measurement range of the instrument by fitting log-normal distributions to the observed data and comparing the measured mass to that expected from the log-normal distribution (e.g., Schwarz *et al.*, 2006). The ratio of the area under the fit to that for the measured data is an estimate of the scaling factor needed to correct the SP2 measurements to account for BC mass outside the SP2 measurement range, assuming the log-normal distribution captures all of the features in the BC mass size distribution. The correction factor does not account for any mass contributed by additional modes in the BC size distribution below or above the SP2 measurement region, such as any contributions by ultra-fine particles to total BC mass below the measurement range. We do not apply such a correction and instead only report BC mass concentrations for the valid measurement range of the instrument as configured for this study (55-400 nm).

2 SP2 DMA Aquadag calibrations

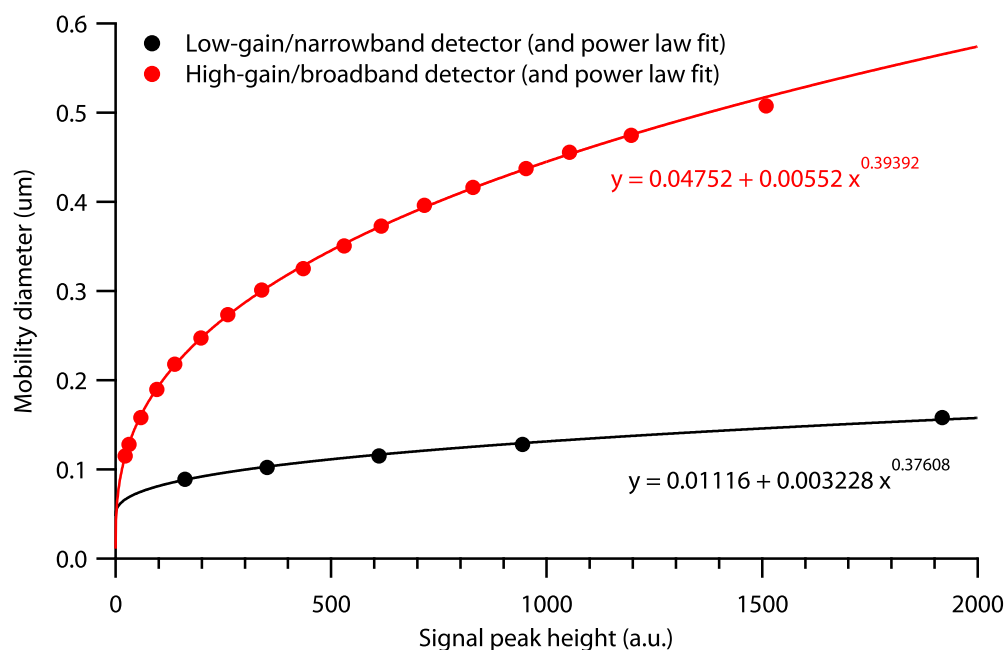


Figure 3: Mobility diameter of aquadag calibration particles plotted as a function of the peak of the frequency distribution of the SP2 detector incandescence peak heights as determined by the instrument manufacturer (DMT). The responses for the low-gain/narrowband detector and high-gain/broadband detector are shown together with the power-law fit used to convert signal height to particle diameter. Mobility diameters were adjusted to black carbon mass using data provided by Moteki and Kondo (personal communication) when calibration was applied to the data. Calibration curves shown here were applied to April (ADIENT) and May (LONGREX) 2008 measurements.

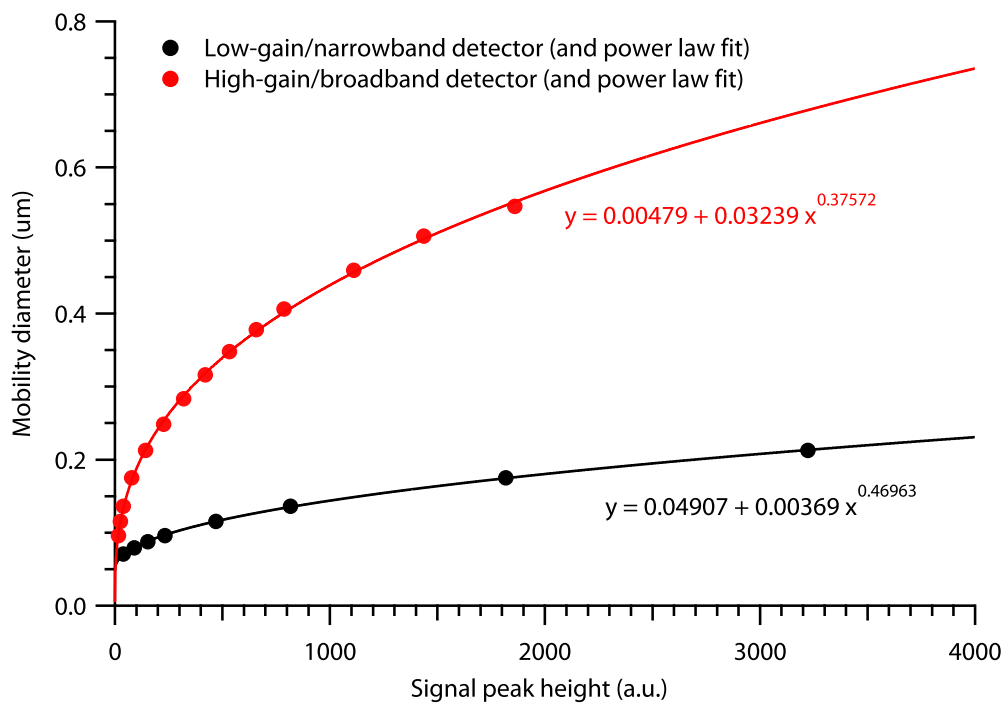


Figure 4: Similar to Figure 1, but for aquadag calibration response curves determined by the instrument manufacturer applied to the September (ADIENT) 2008 SP2 measurements. The maximum incandescence signal increased following a modification to the instrument following a service.

3 Geopotential height fields and FAAM aircraft tracks for flight days

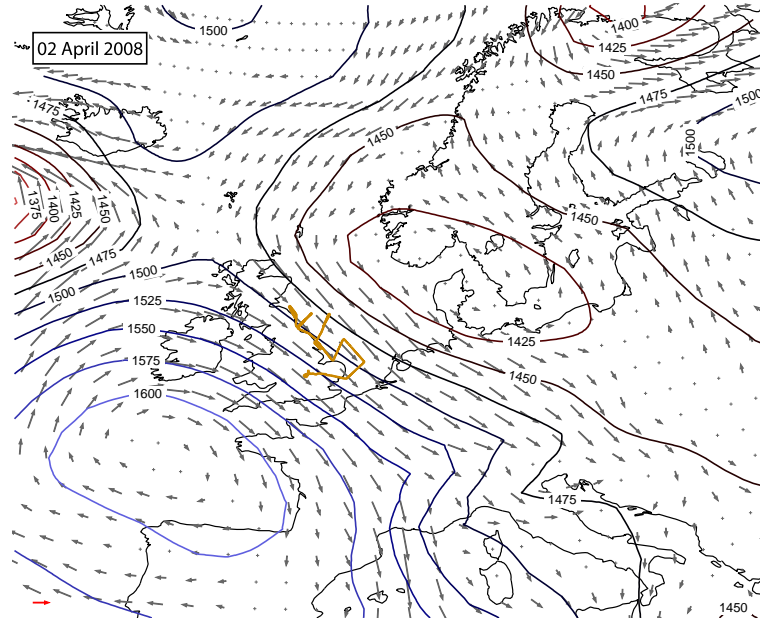


Figure 5: FAAM B355: Map showing meteorological conditions taken from the ECMWF ERA Interim reanalysis and aircraft flight tracks for the day of the FAAM B355 flight (2 April 2008). The 850 hPa geopotential height (m) is shown by solid, shaded contours. The 850 hPa winds are indicated by the grey arrows, with the red arrow in the lower left-hand corner of the map representing a westerly flow at 10 m^{-1} . The flight track of the FAAM aircraft (restricted to altitudes below 3 km) is shown by the thick brown line. The remaining maps show conditions and flight tracks for subsequent flights using the same plotting convention. The flight track of the DLR aircraft is also shown by a thick purple line when it flew on the same day as the FAAM aircraft.

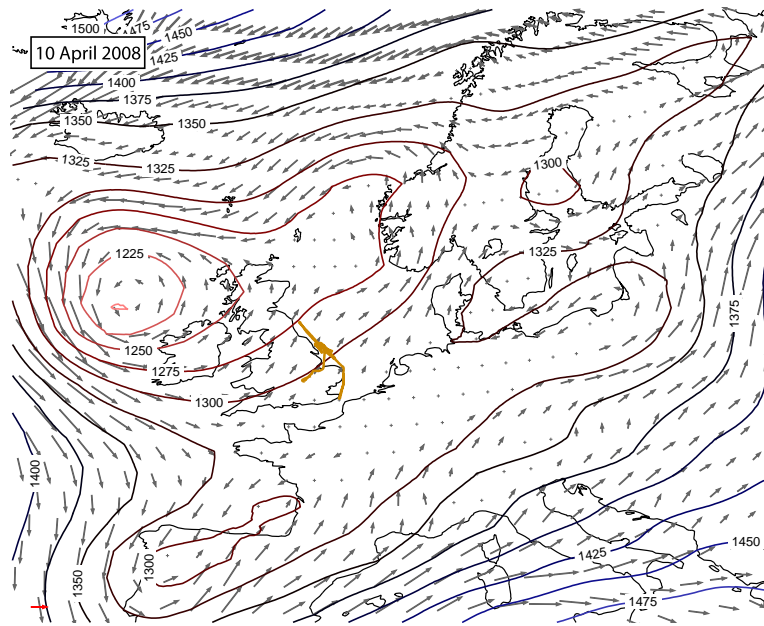


Figure 6: FAAM B356.

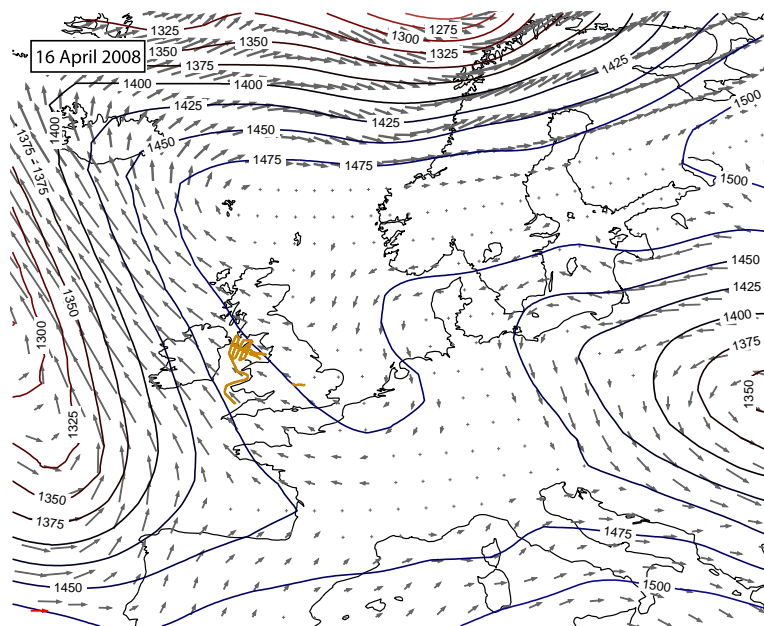


Figure 7: FAAM B356.

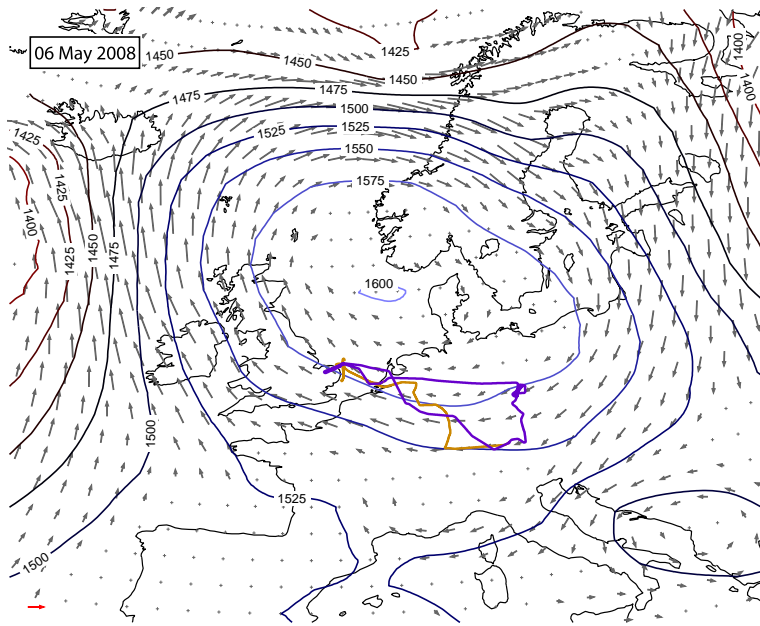


Figure 8: FAAM B366 and DLR 080508b.

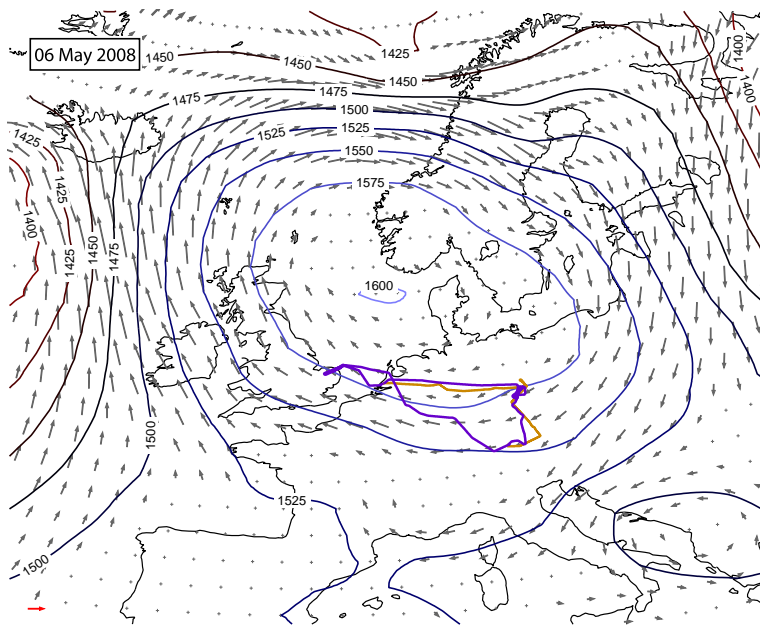


Figure 9: FAAM B363.

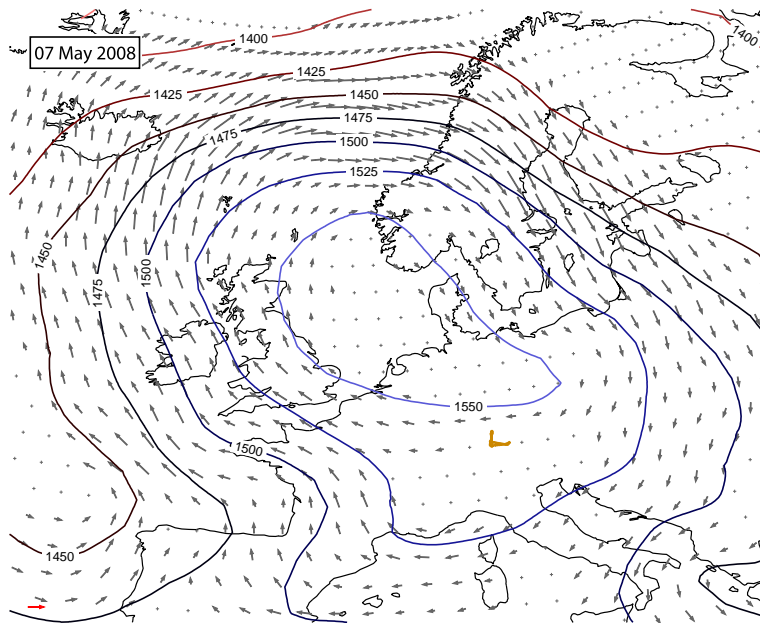


Figure 10: FAAM B364.

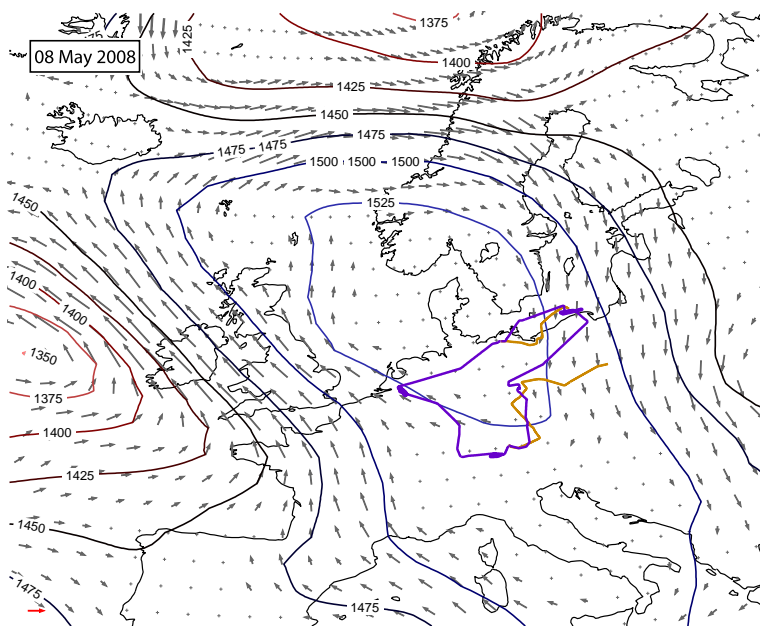


Figure 11: FAAM B365.

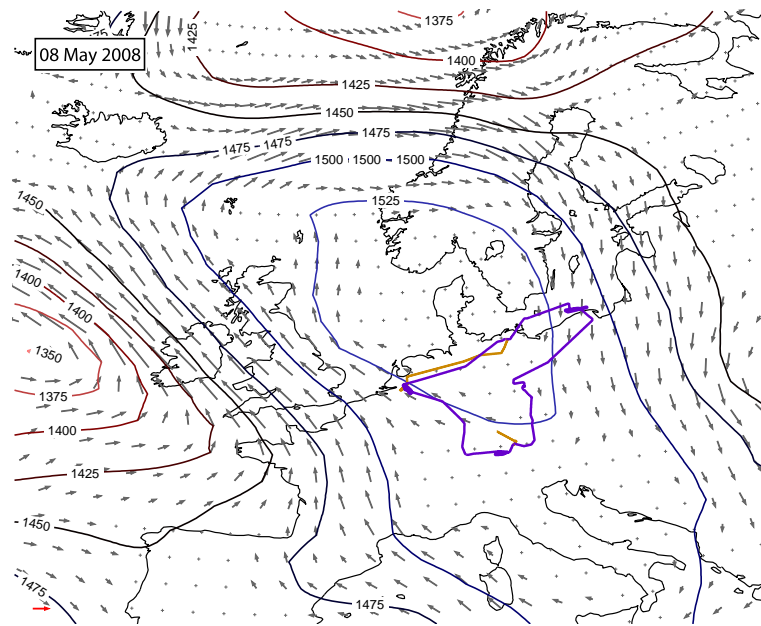


Figure 12: FAAM B366 and DLR 080508b.

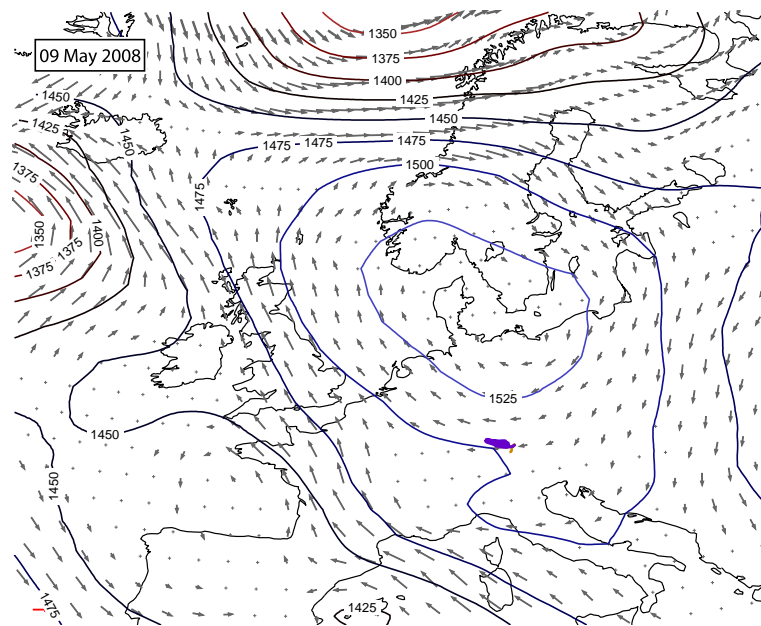


Figure 13: FAAM B367 (inter-comparison flight).

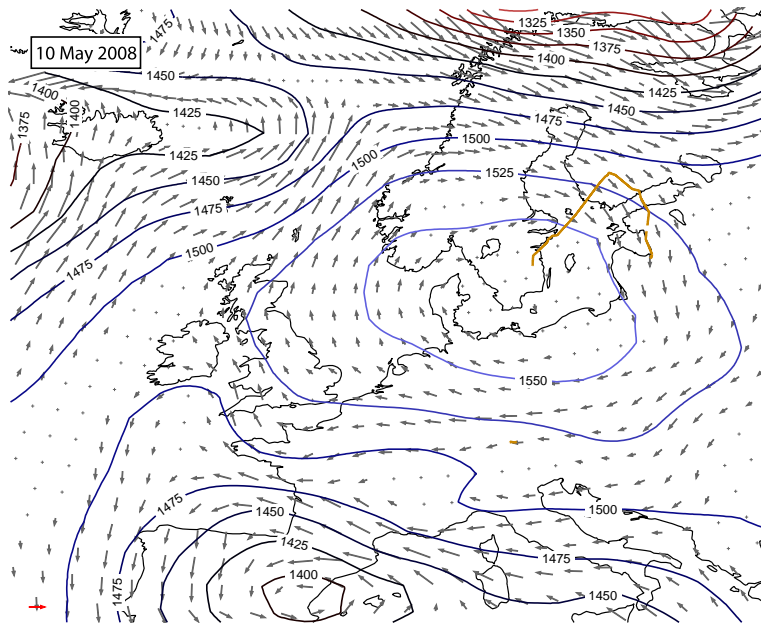


Figure 14: FAAM B368.

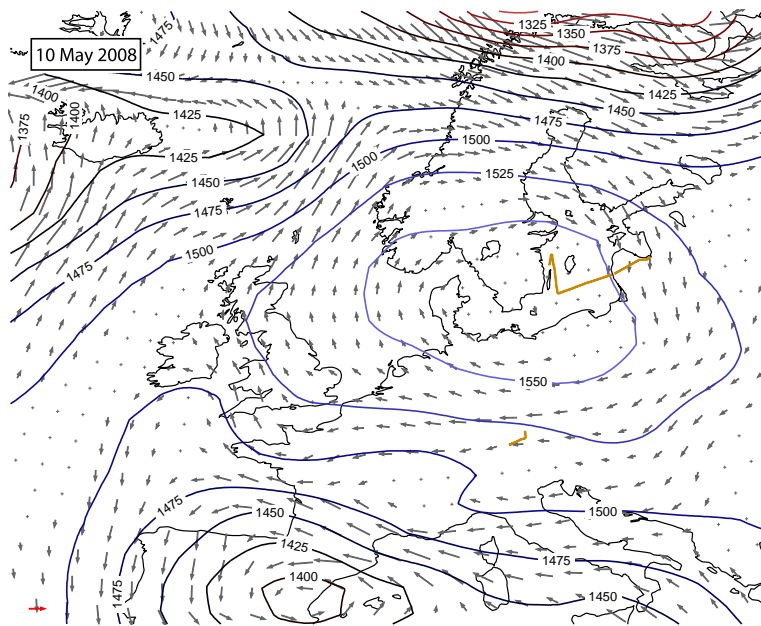


Figure 15: FAAM B369.

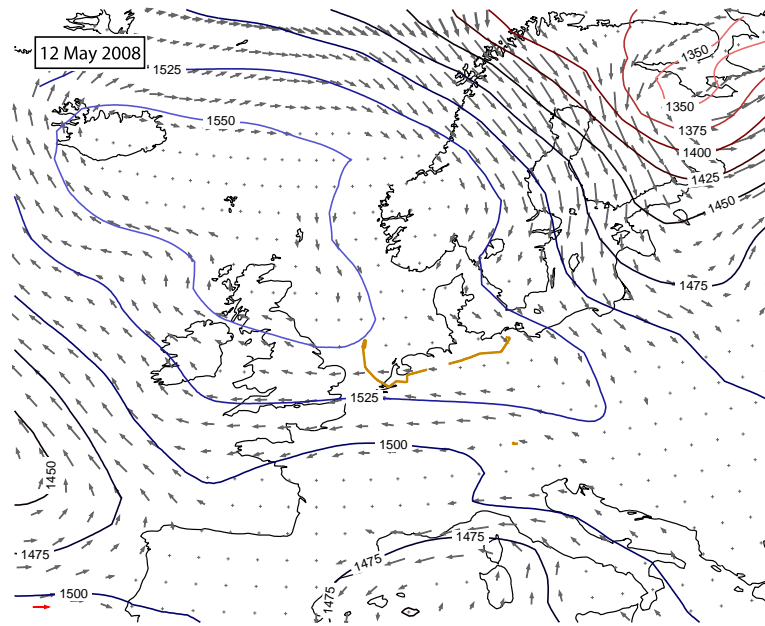


Figure 16: FAAM B370.

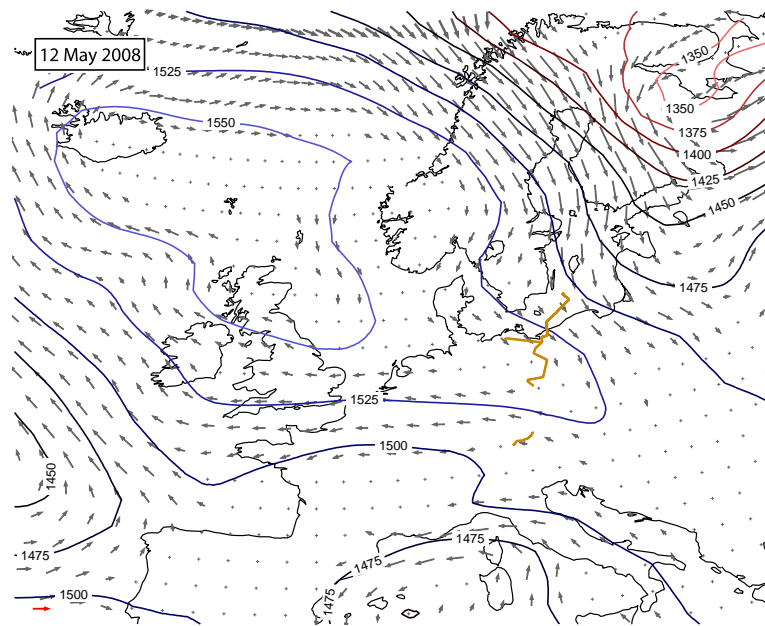


Figure 17: FAAM B371.

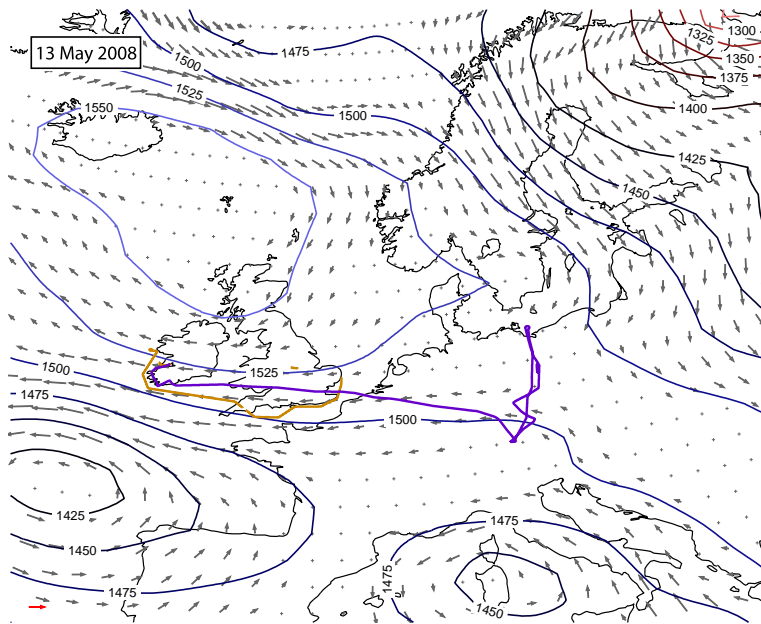


Figure 18: FAAM B373.

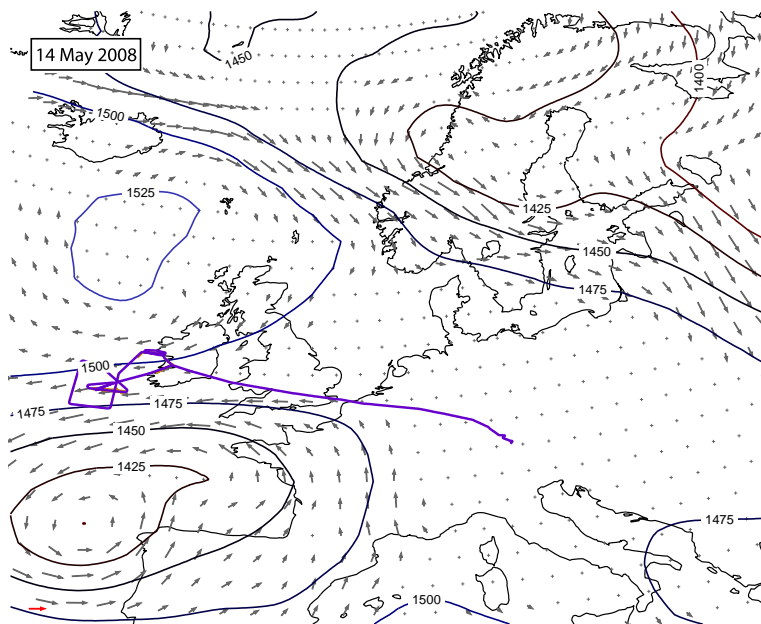


Figure 19: FAAM B374.

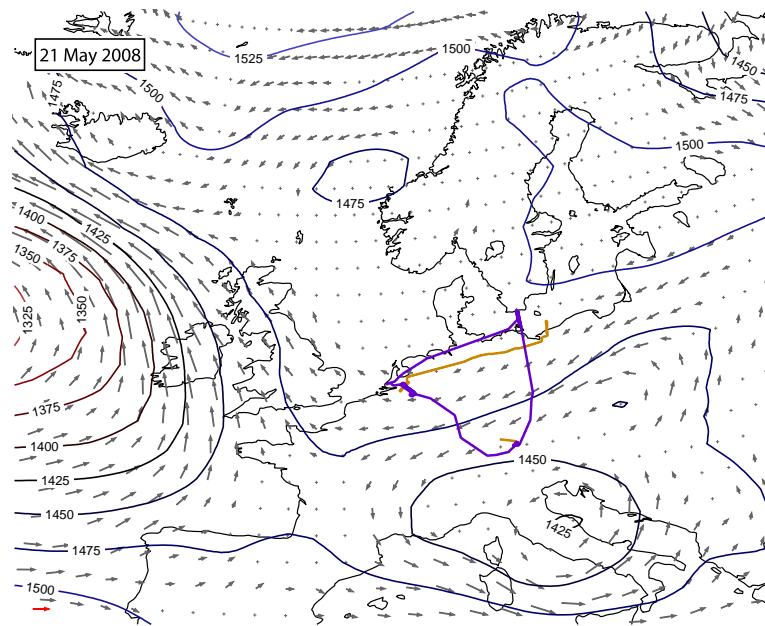


Figure 20: FAAM B379.

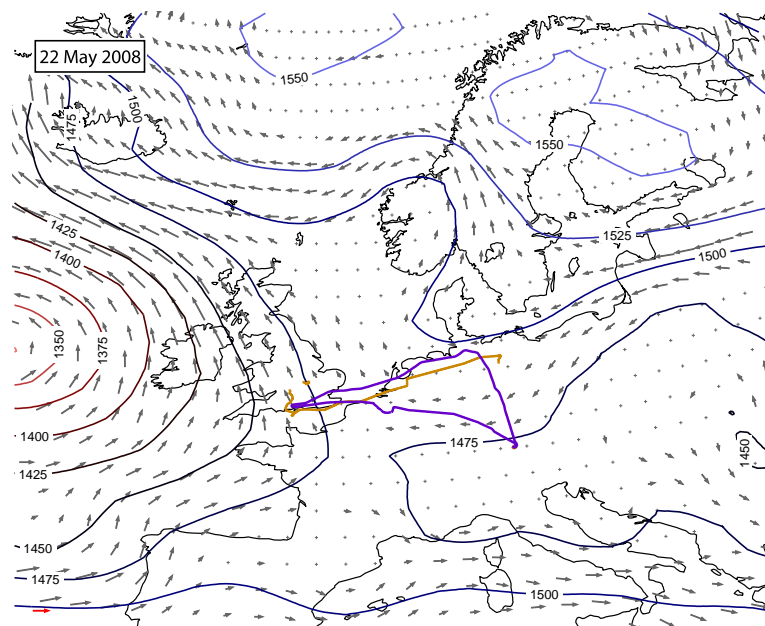


Figure 21: FAAM B380.

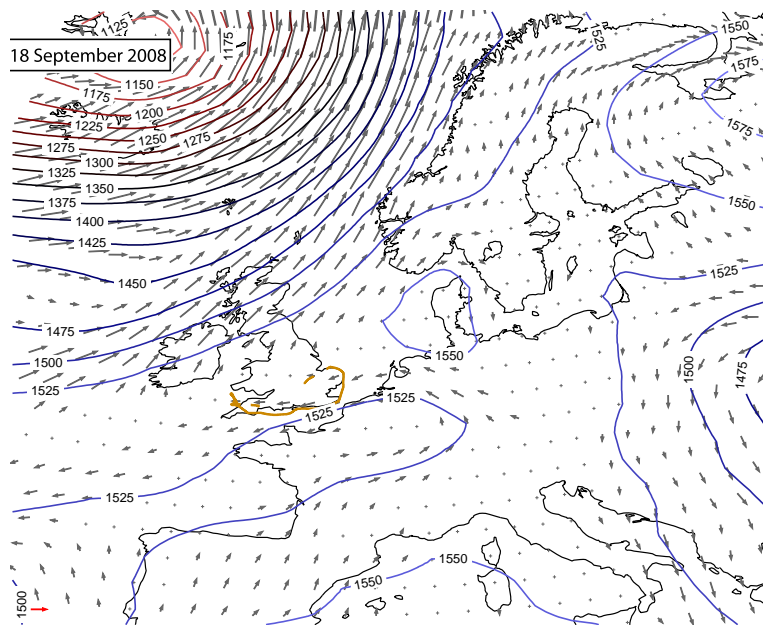


Figure 22: FAAM B401.

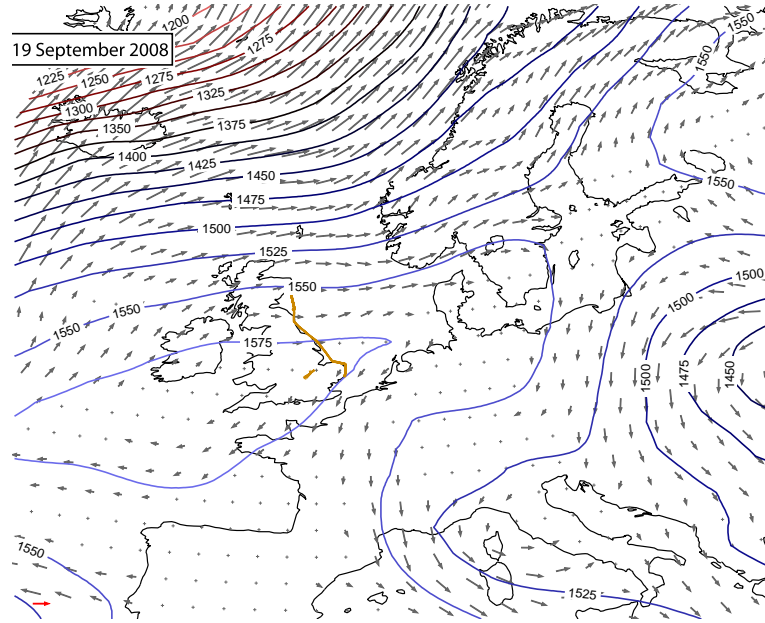


Figure 23: FAAM B402.

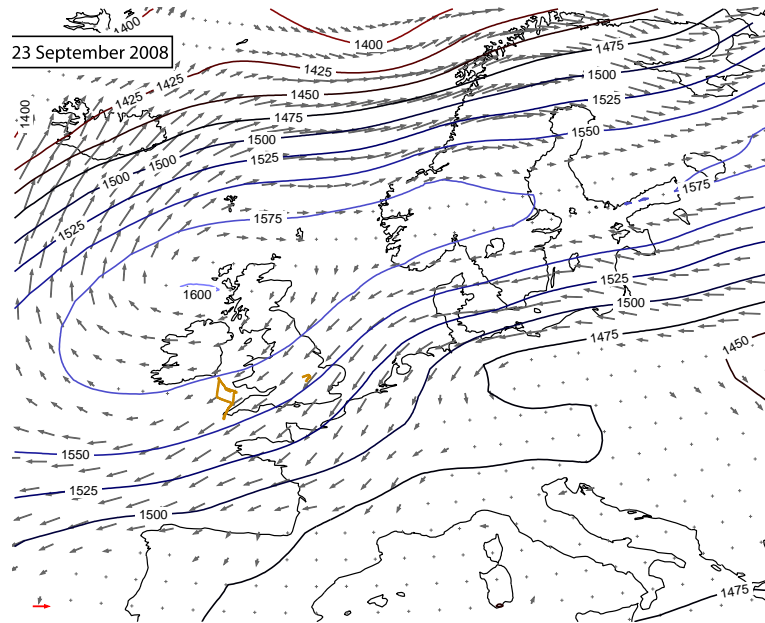


Figure 24: FAAM B404.

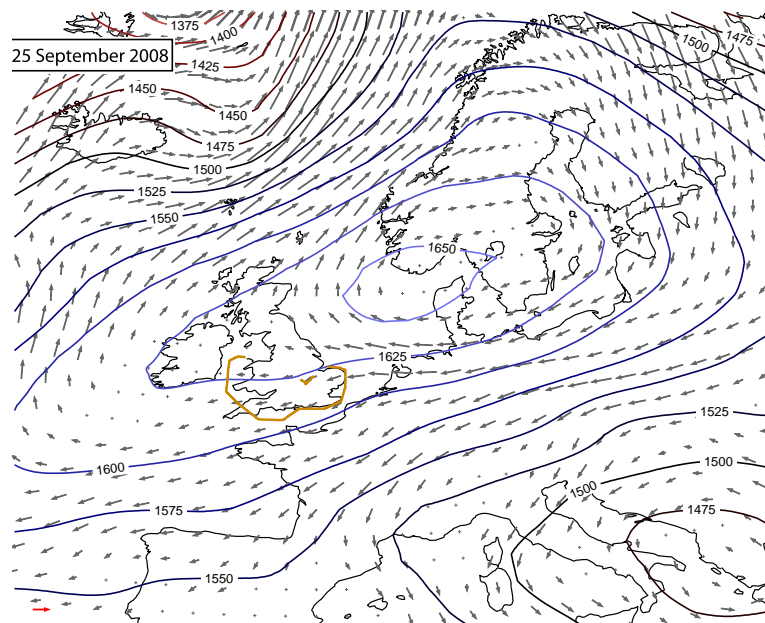


Figure 25: FAAM B406.

References

- Gao, R. S., Schwarz, J. P., Kelly, K. K., Fahey, D. W., Watts, L. A., Thompson, T. L., Spackman, J. R., Slowik, J. G., Cross, E. S., Han, J. H., Davidovits, P., Onasch, T. B., & Worsnop, D. R. 2007. A novel method for estimating light-scattering properties of soot aerosols using a modified single-particle soot photometer. *Aerosol Science and Technology*, **41**(2), 125–135.
- Liu, D., Flynn, M., Gysel, M., Targino, A., Creso, Crawford, I., Bower, K., Choularton, T., Juranyi, Z., Steinbacher, M., Hugglin, C., Curtius, J., Kampus, M., Petzold, A., Weingartner, E., Baltensperger, U., & Coe, H. 2010. Single particle characterization of black carbon aerosols at a tropospheric alpine site in Switzerland. *Atmospheric Chemistry and Physics Discussions*, **10**, 8765–8810.
- Moteki, N., Kondo, Y., Miyazaki, Y., Takegawa, N., Komazaki, Y., Kurata, G., Shirai, T., Blake, D. R., Miyakawa, T., & Koike, M. 2007. Evolution of mixing state of black carbon particles: Aircraft measurements over the western Pacific in March 2004. *Geophysical Research Letters*, **34**(11).
- Schwarz, J. P., Gao, R. S., Fahey, D. W., Thomson, D. S., Watts, L. A., Wilson, J. C., Reeves, J. M., Darbeheshti, M., Baumgardner, D. G., Kok, G. L., Chung, S. H., Schulz, M., Hendricks, J., Lauer, A., Kaercher, B., Slowik, J. G., Rosenlof, K. H., Thompson, T. L., Langford, A. O., Loewenstein, M., & Aikin, K. C. 2006. Single-particle measurements of midlatitude black carbon and light-scattering aerosols from the boundary layer to the lower stratosphere. *Journal of Geophysical Research-Atmospheres*, **111**(D16).
- Shiraiwa, M., Kondo, Y., Moteki, N., Takegawa, N., Sahu, L. K., Takami, A., Hatakeyama, S., Yonemura, S., & Blake, D. R. 2008. Radiative impact of mixing state of black carbon aerosol in Asian outflow. *Journal of Geophysical Research-Atmospheres*, **113**.